Acta Crystallographica Section D
Biological Crystallography
ISSN 0907-4449

Structural analysis of the two horseradish peroxidase catalytic residue variants H42E and R38S/H42E: implications for the catalytic cycle

Kåre Meno,[a] Simon Jennings,[b] Andrew T. Smith,[b] Anette Henriksen[c] and Michael Gajhede[a]*†

[a]Protein Structure Group, Department of Chemistry, University of Copenhagen, Universitetsparken 5, DK-2100 Copenhagen Ø, Denmark, [b]School of Biological Sciences, University of Sussex, Falmer, Brighton, Sussex BN1 9QG, England, and [c]Carlsberg Laboratory, Department of Chemistry, Gamle Carlsberg Vej 10, DK-2500 Valby, Denmark

† Current address: Department of Medical Chemistry, The Royal Danish School of Pharmacy, Universitetsparken 2, DK-2100 Copenhagen Ø, Denmark.

Correspondence e-mail: mig@dfh.dk

Received 18 April 2002
Accepted 23 July 2002

PDB References: H42E HRPC, 4atj, r4atjsf; R38S/H42E HRPC, 1kzm, r1kzmsf.

The crystal structures of horseradish peroxidase C (HRPC) active-site mutants H42E and R38S/H42E co-crystallized with benzhydroxamic acid (BHA) and ferulic acid (FA), respectively, have been solved. The 2.5 Å crystal structure of the H42E–BHA complex reveals that the side-chain O atoms of Glu42 occupy positions that are very similar to the positions of the two side-chain N atoms of the distal histidine in the wild-type HRPC–BHA structure. The mutation disturbs the hydrogen-bonding network extending from residue 42 to the distal calcium ion and results in the absence of the water molecule that is usually ligated to this ion in plant peroxidases. Consequently, the distal calcium ion is six- rather than seven-coordinated. In the 2.0 Å R38S/H42E structure the position of Glu42 is different and no FA is observed in the distal haem pocket. This is a consequence of the absence of the Arg38 side chain, which limits the flexibility of the Glu42 side chain and modulates its acidity, making it unsuitable as a general acid–base catalyst in the reaction cycle. The water ligated to the distal calcium ion is present, showing that the wild-type distal hydrogen-bonding network is preserved. These results show why a glutamic acid residue can substitute for the conserved distal histidine in HRPC and that Arg38 plays a significant role in controlling the positioning and ionization state of the residue at position 42. Furthermore, these structures indicate that changes in the distal cavity are conveyed through the distal hydrogen-bonding network to the distal calcium site.

1. Introduction

Haem peroxidases are present in plants, animals and micro-organisms. They carry out a variety of biosynthesis and degradation reactions using peroxides, in particular H_2O_2, as the source of two oxidizing equivalents. Horseradish peroxidase isoenzyme C (HRPC) is the most thoroughly studied member of the plant peroxidase superfamily and is widely used in the biochemical study of these enzymes (Dunford, 1999). HRPC reacts by a three-step mechanism in which the enzyme is first oxidized by H_2O_2 and then reduced in two sequential one-electron transfer steps by an aromatic donor molecule (AH), typically a small-molecule phenol derivative. The reaction cycle is shown below, where any charges on the haem propionates are ignored.

$$\mathrm{HRPC\{[Fe^{III}]Porph^{2-}\}^{+} + H_2O_2 \xrightarrow{k_1} \underset{\text{Compound I}}{HRPC\{[Fe^{IV}{=}O]Porph^{\bullet-}\}^{\bullet+}} + H_2O}$$

$$\mathrm{HRPC\{[Fe^{IV}{=}O]Porph^{\bullet-}\}^{\bullet+} + AH \xrightarrow{k_2} \underset{\text{Compound II}}{HRPC\{[Fe^{IV}{=}O]Porph^{2-}\}} - H^{+} + A^{\bullet}}$$

$$\mathrm{HRPC\{[Fe^{IV}{=}O]Porph^{2-}\} - H^{+} + AH \xrightarrow{k_3} HRPC\{[Fe^{III}]Porph^{2-}\}^{+} + A^{\bullet} + H_2O}$$

The resting-state ferric HRPC enzyme reacts rapidly with H_2O_2 to form the intermediate termed compound I, which contains oxy-ferryl haem with Fe in the formal oxidation state IV and a porphyrin π-cation radical. Compound I is then reduced by aromatic donor molecules through the intermediate compound II, in which the porphyrin π-cation radical has been reduced, finally returning the enzyme to the resting state (Dunford, 1999). A general mechanism of plant peroxidase substrate oxidation has been proposed on the basis of the crystal structure of HRPC in complex with the *in vivo* substrate ferulic acid {[3-(4-hydroxy-3-methoxyphenyl)-2-propenoic acid], FA; Henriksen *et al.*, 1999}. Furthermore, two possible scenarios for the entire catalytic mechanism have been reviewed recently (Gajhede, 2001).

The mechanism of compound I formation is believed to be similar in all haem peroxidases. Prior to compound I formation, a transient $Fe^{III}-(OOH)^-$ intermediate is formed in which the peroxide proton has been transferred to $N^{\varepsilon 2}$ of the distal histidine (His42 in HRPC; Newmyer & Ortiz de Montellano, 1996). The proton on the distal histidine is then transferred to the hydroxide leaving group, resulting in the generation of a water molecule and compound I. It has been suggested that the distal arginine (Arg38 in HRPC) assists the heterolytic cleavage of the O—O bond by acting as a hydrogen-bond donor to the transient $Fe^{III}-(OOH)^-$ intermediate (Poulos & Kraut, 1980). This is supported by the observation that the rate of compound I formation (k_1) in HRPC is reduced by approximately a factor of 500 if Arg38 is substituted by lysine and by 1200 if Arg38 is substituted by leucine (Smith *et al.*, 1993; Rodriguez-Lopez *et al.*, 1996*a*). The presence of a hydrogen bond between Arg38 N^{ε} and the cyanide N atom in the HRPC–cyanide–FA crystal structure also favours this interpretation (Henriksen *et al.*, 1999).

Upon generation of compound I, Arg38 stabilizes this intermediate (and compound II) by donating a hydrogen bond from N^{ε} to the oxene atom in the ferryl moiety (Edwards *et al.*, 1987; Fülöp *et al.*, 1994; Berglund *et al.*, 2002). Furthermore, Arg38 can promote the binding of phenolic reducing substrates such as FA by donating a hydrogen bond from $N^{\eta 2}$ to the phenolic O atom (Henriksen *et al.*, 1999). When compound I oxidizes AH, a proton is transferred to the distal histidine and the resulting radical ($A^{\cdot}$) dissociates from the distal cavity. When the second reducing substrate is oxidized by compound II the final destination of the accompanying proton transfer is the ferryl oxygen, which is accompanied by proton transfer from the distal histidine to this O atom. This results in the generation of a water molecule, regeneration of resting-state HRPC haem Fe^{III} and reversion of the distal histidine to the uncharged state (Dunford, 1991). The distal histidine is thus acting as a general acid–base catalyst. Both proton transfers from AH are proposed to involve either a water molecule hydrogen bonded to the backbone oxygen of P139 in the distal cavity (Henriksen *et al.*, 1999), a possible second water molecule originating from H_2O_2 during compound I formation (Gajhede, 2001) or both.

The relative contribution of the key distal pocket residues Arg38 and His42 to the rate of compound I formation has been investigated by site-directed mutagenesis experiments in HRPC. The H42L HRPC mutant shows a five orders of magnitude decrease in the rate constant (k_1) for compound I formation (Rodriguez-Lopez *et al.*, 1996*a*). The H42A HRPC mutant is similarly inactive. Addition of exogenous 2-substituted imidazoles to H42A HRPC is found to partially restore catalytic activity, presumably by providing an alternative catalytic base (Newmyer & Ortiz de Montellano, 1996). These experiments have been generally accepted as confirming the essential role of His42 as the proton acceptor for incoming substrates, including H_2O_2 and HCN. The efficiency of a surrogate catalytic histidine residue has also been explored by means of the F41H/H42A (Savenkova *et al.*, 1996) and R38H/H42V (Savenkova *et al.*, 1998) HRPC double mutants, which allow partial restoration of compound I formation rates, with rate constants for compound I formation being 3–4 orders of magnitude slower than the wild type. Hence, the precise location of the catalytic base does not appear to be essential in order to attain an intermediate (10^3–$10^4\ M^{-1}\ s^{-1}$) rate of compound I formation ($k_1 \simeq 10^7\ M^{-1}\ s^{-1}$ for wild-type HRPC). Analysis of the N70V and N70D HRPC mutants has shown that loss of the hydrogen bond between His42 and Asn70 results in a decrease in the basicity of His42 and a decrease in the rate of compound I formation (Nagano *et al.*, 1996; Mukai *et al.*, 1997). Mutagenesis experiments conducted in HRPC (Rodriguez-Lopez *et al.*, 1996*a*,*b*) suggest that the catalytic arginine (Arg38) is not absolutely essential for compound I formation in plant peroxidases. Arg38 enhances the efficiency of the reaction by increasing the affinity of the enzyme for ligands including H_2O_2 and by enhancing the rate of O—O bond cleavage (Rodriguez-Lopez *et al.*, 1996*b*) (as described above). All these experiments concur that the distal histidine is the most important residue for maintenance of peroxidase activity.

Study of the H42E HRPC mutant was prompted by the discovery of a glutamic acid residue (Glu183) in the active site of chloroperoxidase (CPO; Sundaramoorthy *et al.*, 1995). CPO is a fungal peroxidase from an unrelated haem-peroxidase superfamily capable of rapid compound I formation (Sun *et al.*, 1994), but also with a different reducing-substrate oxidation pattern. The glutamic acid residue has been implicated as the catalytic base in compound I formation. Notably, CPO lacks the catalytic arginine residue (Arg38 in HRPC) characteristic of the plant peroxidases. Previous characterization of the H42E HRPC mutant (Tanaka *et al.*, 1997) has shown that the presence of a glutamic acid residue at position 42 allows a rate of compound I formation ($k_1 = 4.9 \times 10^3\ M^{-1}s^{-1}$) similar to that achieved with a surrogate histidine (described above) and a factor of 50 higher than that observed in a H42Q HRPC mutant ($k_1 = 9.6 \times 10^1\ M^{-1}\ s^{-1}$). Interestingly, this is still 500-fold lower than the rate catalysed by CPO ($k_1 = 2.3 \times 10^6\ M^{-1}\ s^{-1}$; Sun *et al.*, 1994). The inability of a Glu at position 42 to fully replace the functional role of the distal histidine has previously been ascribed to its decreased basicity relative to the histidine and supposed improper positioning owing to the lack of a hydrogen bond with Asn70 (Tanaka *et al.*, 1997), but the structural details have not hitherto been investigated.

In this crystallographic study, the H42E HRPC (denoted H42E) and R38S/H42E HRPC (denoted R38S/H42E) mutant structures co-crystallized with benzhydroxamic acid (BHA) and FA, respectively, are reported. The chemical and structural background for the established ability of a glutamic acid to partly replace histidine in HRPC catalysis is hereby addressed.

2. Materials and methods

2.1. Protein expression, purification and crystallization

Site-directed mutants of HRPC were constructed as described previously (Smith *et al.*, 1992). Expression, refolding and purification have been described elsewhere (Smith *et al.*, 1990).

H42E mutant crystals were grown by co-crystallization of recombinant H42E and BHA as described for the wild-type enzyme (Henriksen *et al.*, 1998). Hanging drops containing 3 µl of 5.7 mg ml^{-1} H42E, 3 µl reservoir solution and 1 µl of 2.5 m*M* BHA were equilibrated against 500 µl reservoir solution containing 1.2 *M* $NH_4H_2PO_4$, 0.1 *M* cacodylate buffer pH 6.5 at 283 K. The crystal used for data collection was monoclinic, crystallizing in space group $P2_1$ with unit-cell parameters a = 74.9, b = 62.3, c = 78.2 Å, β = 104.3°. Two molecules were present in the asymmetric unit, related by a non-crystallographic twofold axis (Henriksen *et al.*, 1998).

R38S/H42E mutant crystals were grown by co-crystallization of recombinant R38S/H42E and FA as described for the wild-type enzyme (Henriksen *et al.*, 1999). Hanging drops containing 3 µl of 4.9 mg ml^{-1} R38S/H42E, 3 µl reservoir solution and 2 µl saturated FA in 2-propanol were equilibrated against 500 µl reservoir solution containing 20%(*w*/*v*) PEG 8000, 0.2 *M* calcium acetate and 0.1 *M* cacodylate buffer pH 6.5 at 283 K. Prior to data collection, the crystal was soaked briefly in a cryoprotective solution containing 35% PEG 8000, 0.1 *M* cacodylate buffer pH 6.5 and shock-frozen in liquid nitrogen. Data were collected at 120 K; the space group was $P2_12_12_1$, with unit-cell parameters a = 40.4, b = 66.7, c = 117.1 Å. These crystals contained only one molecule in the asymmetric unit.

2.2. X-ray data collection and reduction

Data were collected from a single H42E crystal mounted in a glass capillary using a Rigaku R-AXIS IIC image-plate system with a Rigaku RU-200 rotating-anode generator operating at 180 mA and 50 kV as the source of Cu $K\alpha$ X-rays. The system was equipped with a graphite monochromator and a 0.5 mm collimator. A total of 60 successive frames were collected with 2° oscillation for each frame. The crystal-to-detector distance was 100 mm. Data collection took place at room temperature, with an exposure time of 60 min for each frame.

The R38S/H42E data were collected at beamline ID-14 at the European Synchrotron Radiation Facility (ESRF) on a frozen crystal mounted in a cryoloop. A MAR Research CCD detector positioned 150 mm from the crystal was used for data collection. A total of 92 successive frames were collected with 1° oscillation for each frame.

Table 1
Summary of the data-collection and refinement results.

Values in parentheses refer to the highest resolution shell.

	H42E	R38S/H42E
Data collection		
Wavelength (Å)	1.54	0.934
Resolution range (Å)	45–2.5 (2.54–2.50)	20–2.0 (2.03–2.00)
Space group	$P2_1$	$P2_12_12_1$
Reflections	79639	122607
Unique reflections	23302	21058
Completeness (%)	95.4 (95.4)	95.1 (95.8)
R_{sym}†	0.132 (0.390)	0.059 (0.185)
Redundancy	3.4	5.8
$I > 3\sigma(I)$ (%)	61.8 (33.9)	79.3 (48.2)
Refinement		
Unique reflections ($I > 0$)	22747	20468
R_{work}‡	0.161	0.168
R_{free}‡	0.192	0.203
Protein atoms	2385	2364
Heterogen atoms§	55	50
Water molecules	152	295
R.m.s.d. bond length¶ (Å)	0.006††	0.005‡‡
R.m.s.d. bond angle¶ (°)	1.1††	1.2‡‡
Mean protein B factor (Å^2)	16.9	15.7
Mean water B factor (Å^2)	26.4	26.8
Estimated coordinate error from Luzzati plot (Å)	0.22 (0.27)††	0.18 (0.23)‡‡
Ramachandran plot (non Gly and Pro)§§, residues in		
Most favoured regions (%)	89.0	89.3
Additional allowed regions (%)	10.7	10.4
Disallowed regions (%)	0.0	0.0

† $R_{sym} = \sum_h \sum_i |I_i(h) - \langle I(h)\rangle| / \sum_h \sum_i I_i(h)$. ‡ $R_{work} = R_{free} = \sum_h ||F_o(h)| - k|F_c(h)|| / \sum_h |F_o(h)|$. § Haem, calcium, cacodylate and BHA/FA. ¶ From ideal values. †† Calculated with the program *X-PLOR* (Brünger, 1992*b*). ‡‡ Calculated with the program *CNS* (Brünger *et al.*, 1998). §§ Calculated with the program *PROCHECK* (Laskowski *et al.*, 1993).

For both data sets, autoindexing and integration of intensities were performed using the program *DENZO*, whereas the data were averaged and scaled with the *SCALEPACK* program (Otwinowski, 1993). Statistics from the data processing are listed in Table 1. The reason for the lower R_{sym} observed for R38S/H42E compared with H42E was the intrinsic superior crystal quality of the orthorhombic crystal form compared with the monoclinic crystal form.

2.3. Structure solution and refinement

The H42E data showed that the mutant crystal was practically identical to the wild-type HRPC–BHA crystal (Henriksen *et al.*, 1998), so this structure, including protein, haem, BHA, calcium ions and water, was used for initial map calculations without performing a molecular-replacement search. Refinement of the atom positions utilizing conjugate-gradient minimization and slow-cool simulated-annealing minimization was performed with the *X-PLOR* program package (version 3.851; Brünger, 1992*b*). 10% of the data was omitted from the refinement and used as a test set (Brünger, 1992*a*). Bulk-solvent correction was applied (Jiang & Brünger, 1994) as well as strict NCS. Individual but restrained B factors were refined in *X-PLOR*. $2F_o - F_c$ and $F_o - F_c$ electron-density maps were calculated in *X-PLOR* (Read, 1986;

Kleywegt & Brünger, 1996) and used for model corrections in *O* (Jones *et al.*, 1991). Water molecules were retained in the model if they returned $2F_o - F_c$ electron density and obeyed hydrogen-bonding criteria. Iterative cycles of model building in *O* were followed by refinement in *X-PLOR*. In an attempt to resolve the orientations of $O^{\delta1}$ and $N^{\delta2}$ in the Asn70 side chain, refinements were performed with H atoms and electrostatic forces included for both orientations of Asn70. This resulted in small and insignificant changes in the area surrounding this residue, as could be expected with a 2.5 Å resolution data set. The structure was therefore refined using the default approach without H atoms and charges.

Since the R38S/H42E crystal geometry was almost identical to the wild-type FA crystal form (Henriksen *et al.*, 1999), phases from that structure were obtained by Fourier synthesis as described above, with the difference that only protein, haem and calcium ions were included in the starting model. 5% of the data was used as a test set. Iterative cycles of model building in *O* were followed by refinement in *CNS* (Brünger *et al.*, 1998). The refinement was performed using amplitudes and bulk-solvent correction; negative intensities were assigned an amplitude of zero. Simulated annealing was used in the first refinement cycle to remove phase bias and the remaining refinement cycles were performed using conjugated-gradient minimization. The relative occupancies of residues in two conformations (Ile53, Arg82, Cys91, Ser161, Ser188, Ser265, Cys301 and Val304) were refined, but the sum was not restricted to equal 1.0. Restrained individual *B* factors were refined in *CNS* (Brünger, 1992*a*; Pannu & Read, 1996). In each refinement cycle, water molecules were added automatically to the model and evaluated by the resulting electron density and the real-space correlation using *CNS*. A few water molecules were added manually and these were confirmed with *CNS* by the same method. All water molecules were checked manually in the final model for potential hydrogen bonds and $\geq 1\sigma$ $2F_o - F_c$ electron density. $2F_o - F_c$ and $F_o - F_c$ electron-density maps were calculated using *CNS* (Read, 1986; Kleywegt & Brünger, 1996; Brünger *et al.*, 1997) and these maps were used for the manual model corrections in *O*. More than 20σ $F_o - F_c$ electron density was observed on the surface of R38S/H42E between residues Arg283 and Asn286. A cacodylate ion was inserted into this density and this yielded a tetrahedral $2F_o - F_c$ density with only $\sim 3\sigma$ residual $F_o - F_c$ density and *B* factors below 25 $Å^2$ for all atoms. Cacodylate was used in the crystallization buffer, so the presence of this ion in the R38S/H42E crystal structure is of no biological significance.

Engh and Huber parameters were used to restrain the protein geometry in both mutants (Engh & Huber, 1991). Statistics from the structure refinement are listed in Table 1.

3. Results and discussion

3.1. Overall protein fold and comparison with the wild type

All 308 amino-acid residues of mature HRPC except the C-terminal Ser308 are visible in the H42E electron density. Furthermore, a methionine (residue 0) added to the N-terminus for expression purposes is observed. For the R38S/H42E structure 306 residues are visible. No electron density was observed for the two C-terminal residues Asn307 and Ser308, presumably because of flexibility. The extra methionine residue at the N-terminus described for H42E was not seen in R38S/H42E.

The overall fold of the H42E and R38S/H42E mutants is unchanged compared with the structure of the wild-type protein (Gajhede *et al.*, 1997; Fig. 1). The overall root-mean-square deviation between the positions of the C^{α} atoms of residues 1–306 is 0.13 Å on superposition of H42E and wild-type HRPC–BHA (Henriksen *et al.*, 1998) and 0.17 Å on superposition of R38S/H42E and wild-type HRPC–FA (Henriksen *et al.*, 1999). The value obtained when superimposing H42E and R38S/H42E is 0.34 Å. The Ramachandran plot of both mutants shows no residues in the disallowed regions and only one residue, Thr288, in the generously allowed regions. The same is observed in the wild-type HRPC–BHA and HRPC–FA structures.

There are four disulfide bridges in HRPC, which are conserved in the family of secreted peroxidases from higher plants. The disulfide bridge between Cys97 and Cys301 observed in all other HRPC crystal structures is broken in

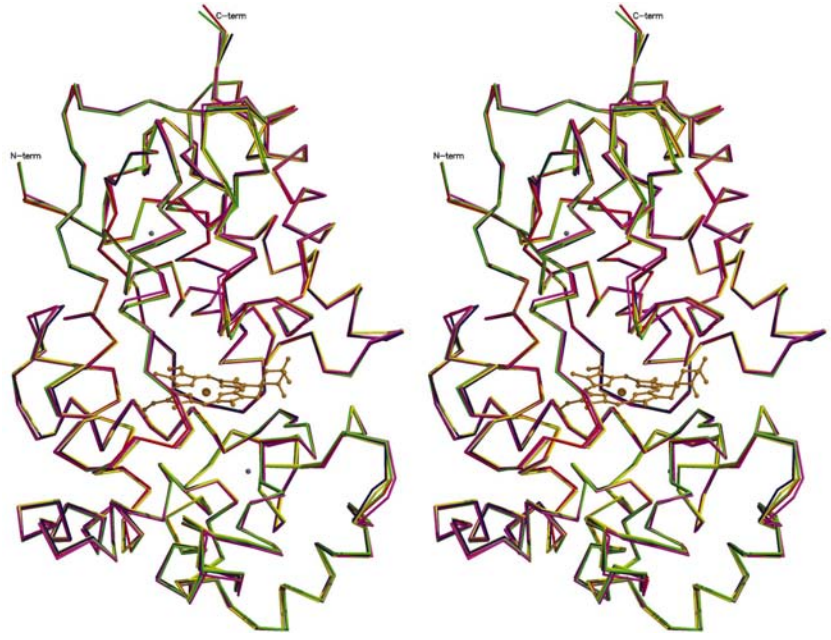

Figure 1
Superimposed stereo C^{α} trace of HRPC (magenta; Gajhede *et al.*, 1997), HRPC–BHA (red; Henriksen *et al.*, 1998), HRPC–FA (blue; Henriksen *et al.*, 1999), H42E (green) and R38S/H42E (yellow). The haem and the proximal (bottom) and distal (top) calcium ions (grey spheres) from the HRPC–FA structure are shown. This figure was produced with the programs *MOLSCRIPT* (Kraulis, 1991) and *RASTER3D* (Merritt & Murphy, 1994)

the R38S/H42E structure. The structure was therefore refined without the restraint of a disulfide bridge between these cysteine residues. The electron density indicates the presence of two conformations of Cys301, while Cys97 is placed in virtually the same position as in the wild-type HRPC–FA structure. Cys301 conformation 1 represents basically the same overall side-chain rotamer as in the wild type, but the entire residue has moved and the distance between Cys301 S^{γ} and Cys97 S^{γ} is 2.9 Å, compared with 2.0 Å in the wild type. Conformation 2 represents another side-chain rotamer and S^{γ} is pointing away from Cys97. In both conformations the distance between the S^{γ} atoms is too great for a disulfide bond, since the ideal distance is 2.0 Å. The reason for this breakage is presumably radiation damage caused by the high intensity at ESRF, which is known to damage even cryocooled protein crystals (Burmeister, 2000). The two conformations then represent an average over space and time of the transition from a cystine residue to two free cysteine residues (or radicals). The freezing presumably prevented major rearrangements as a result of this breakage.

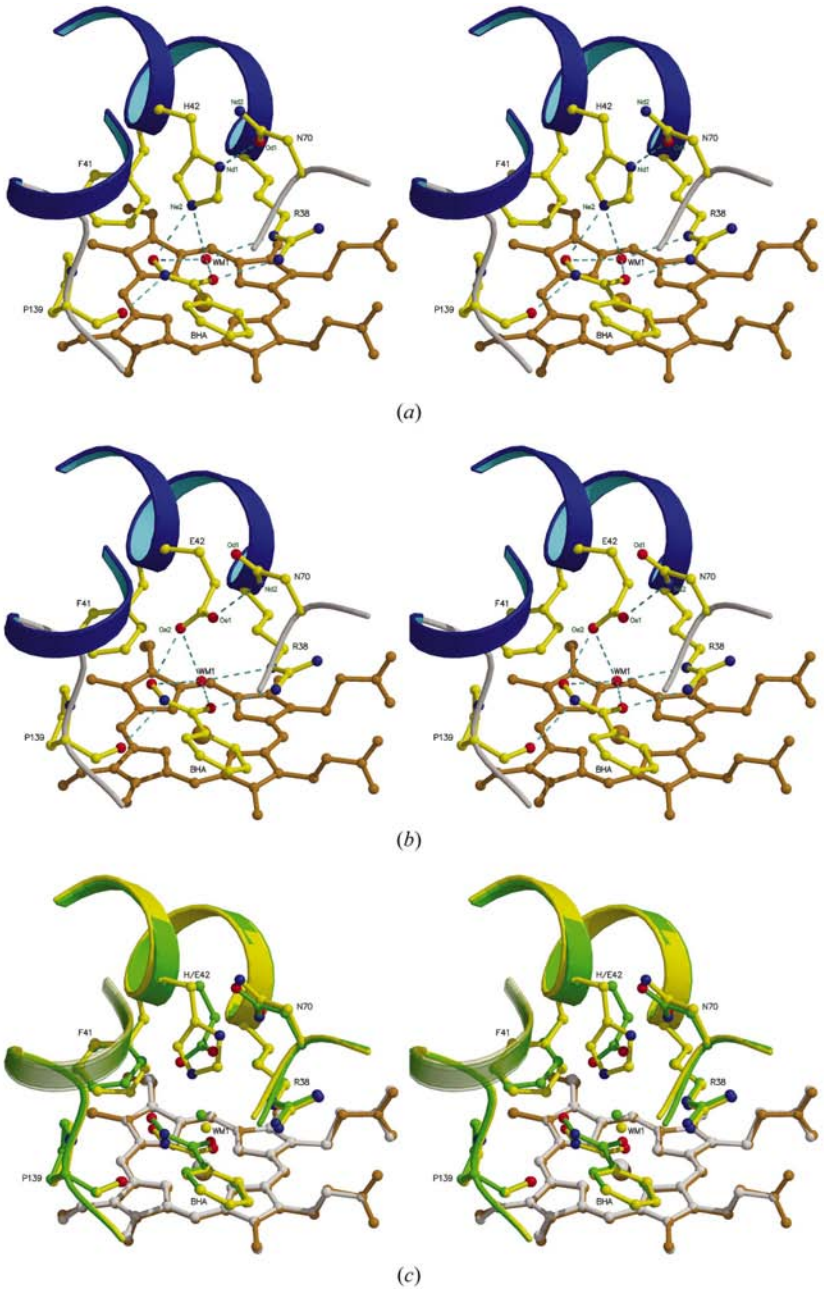

Figure 2
Important residues surrounding the distal haem pocket in the wild-type HRPC–BHA (*a*) (Henriksen *et al.*, 1998) and H42E (*b*) structures. In (*c*), the two structures are superimposed with the C atoms in yellow and green for the wild type and H42E, respectively. The wild-type haem is in brown, while the H42E haem is in grey. The WM1 water molecule has the same colour as the C atoms in the corresponding structure. Hydrogen bonds with a maximum length of <3.5 Å between selected atoms are shown by broken lines in (*a*) and (*b*). Residues are labelled with single-letter codes. In the atom names, d = δ and e = ε. This figure was produced with the programs *MOLSCRIPT* (Kraulis, 1991) and *RASTER3D* (Merritt & Murphy, 1994).

3.2. Distal haem pocket, catalytic residues and bound substrates

The refined H42E structure shows that a mutation of the distal histidine residue to a glutamic acid does not cause major changes in the positions of the surrounding amino-acid residues or of the BHA molecule present in the distal cavity. BHA was added during crystallization to give the simpler monoclinic crystal form with two molecules in the asymmetric unit instead of the six molecules observed in the crystal of the uncomplexed enzyme (Gajhede *et al.*, 1997). In the wild-type HRPC–BHA complex (Henriksen *et al.*, 1998) BHA makes extensive hydrogen-bonding contacts with His42, Arg38, Pro139 and a conserved water molecule (denoted WM1). Figs. 2(*a*) and 2(*b*) compare the hydrogen-bonding interactions in the wild type and H42E BHA complexes. Glu42 is still able to form hydrogen bonds with the same atoms in the distal cavity (except Asn70 $O^{\delta1}$ as described below). In order to conserve these hydrogen bonds, the BHA molecule, WM1 and Arg38 all seem to compensate for the replacement of the histidine side chain by adjustments of their positions (Fig. 2*c*). The hydrophobic interactions are also slightly affected by the –mutation, exemplified by a small rotation (22°) of the Phe41 side chain.

The ionization state of the Glu42 side chain is the key to understanding changes in its hydrogen-bonding possibilities. The hydrogen bond to the important anchor residue Asn70 assures that His42 is protonated on $N^{\delta1}$ and positions His42 $N^{\varepsilon2}$ above the haem in the wild type. In this way, His42 $N^{\varepsilon2}$ can function as a proton acceptor. The close proximity of

Glu42 $O^{\varepsilon1}$ and the Asn70 side chain (2.7 Å) in the H42E structure suggests the presence of a hydrogen bond. Glu42 $O^{\varepsilon1}$ will only be able to function as a hydrogen-bond donor in the protonated state, as His42 $N^{\delta1}$ does in the resting-state wild-type structure. The pH dependence of the guaiacol oxidation activity of the H42E mutant shows that the activity increases consistently in the acidic and neutral pH regions and reaches its maximum value in the basic region (Tanaka *et al.*, 1996). Since Glu42 will be unable to function as a proton acceptor in the protonated state, this suggests that the described pH dependency corresponds to a deprotonation of Glu42. Hence, Glu42 is expected to be protonated in the crystal structure, given that the pH in the crystallization buffer was slightly acidic (pH 6.5). The question then remains as to whether the proton is located on Glu42 $O^{\varepsilon1}$ or $O^{\varepsilon2}$. If it is located on $O^{\varepsilon1}$, Glu42 can donate a hydrogen bond to Asn70 $O^{\delta1}$. If, on the other hand, it is placed on $O^{\varepsilon2}$, Glu42 can donate a hydrogen bond to WM1, but then Glu42 is unable to form a hydrogen bond with the Asn70 side chain. In this case, it is plausible that the Asn70 side chain is rotated relative to the wild-type structures, resulting in a hydrogen bond between Asn70 $N^{\delta2}$ and Glu42 $O^{\varepsilon1}$ as depicted in Fig. 2(*b*). This rearrangement has the minor disadvantage that Asn70 $O^{\delta1}$ is placed 3.0 Å from the backbone O atom of Glu64. It is not possible from the H42E crystal structure to determine whether Asn70 $O^{\delta1}$ or $N^{\delta2}$ is pointing towards Glu42 (see §2.3), mainly because the electron densities of oxygen and nitrogen are indistinguishable by X-ray crystallography at this resolution. The position of WM1 is significantly altered (0.6 Å) in H42E compared with the wild-type HRPC–BHA structure (Fig. 2*c*). WM1 has moved away from the haem iron, so the WM1–iron distance is 2.9 Å instead of 2.6 Å and it is located closer to the Phe41 and Glu42 side chains. This suggests that the WM1 lone pair interacting with the haem iron in the wild type is engaged in a hydrogen bond with Glu42 in the H42E variant. The other WM1 lone pair is part of the hydrogen bond to Arg38 N^{ε}. In this way WM1 could accept a hydrogen bond from the protonated Glu42 $O^{\varepsilon2}$ atom, thus explaining the altered position of WM1 in H42E and supporting the suggestion that the proton is located on $O^{\varepsilon2}$.

Evidence for a 180° rotation around the $C^{\beta}-C^{\gamma}$ bond (the χ_2 angle) in the Asn70 side chain under certain conditions comes from kinetic studies on H42E. The significantly faster rate of compound I formation (k_1) by H42E compared with the H42Q HRPC mutant at pH 7.0 (Tanaka *et al.*, 1997), together with the pH dependency of the guaiacol oxidation activity of H42E (Tanaka *et al.*, 1996), implies that Glu42 functions as a general acid–base

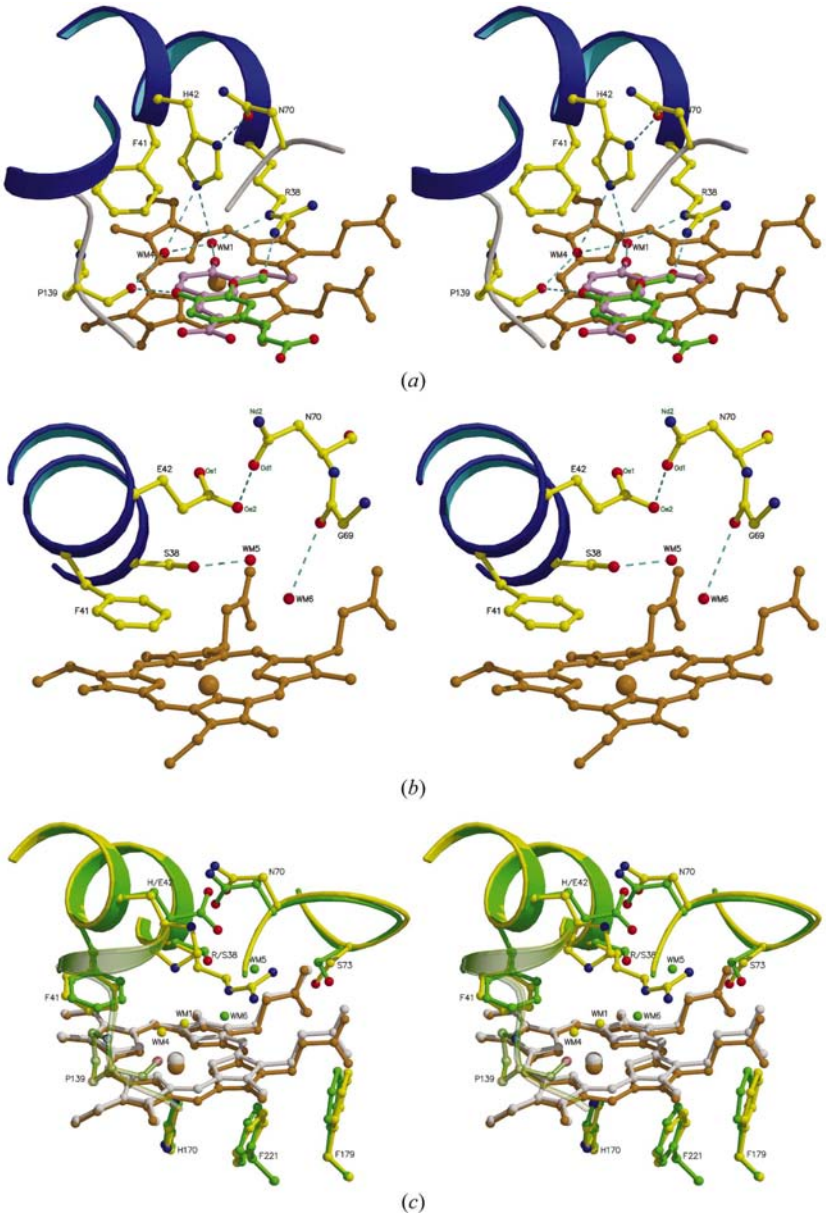

Figure 3
Important residues surrounding the haem in the wild-type HRPC–FA (Henriksen *et al.*, 1999) (*a*) and R38S/H42E (*b*) structures. For the wild-type structure, the FA binding mode with the carboxylate group pointing in to the distal pocket (FA3) has been omitted for clarity, since this represents a biologically irrelevant conformation (Henriksen *et al.*, 1999). The FA1 and FA2 binding modes are in purple and green, respectively. In R38S/H42E no FA is observed in the pocket; instead, this position is occupied by a disordered water molecule (WM6). A water molecule strongly hydrogen bonded to Ser38 is located in the area occupied by Arg38 in the wild type (WM5). The two structures are superimposed in (*c*) with C atoms in yellow and green for the wild type and R38S/H42S, respectively. The wild-type haem is in brown, while the R38S/H42E haem is in grey. The water molecules have the same colour as the C atoms in the corresponding structure. Hydrogen bonds with a maximum length of <3.5 Å between selected atoms are shown by broken lines in (*a*) and (*b*). Residues are labelled with single-letter codes. In the atom names d = δ and e = ε. This figure was produced with the programs *MOLSCRIPT* (Kraulis, 1991) and *RASTER3D* (Merritt & Murphy, 1994).

catalyst at neutral and basic pH. In the active state, the Glu42 residue must be a negatively charged hydrogen-bond acceptor. It is therefore likely that the Asn70 side chain is rotated in the active H42E enzyme in order to maintain the positioning of the deprotonated Glu42 side chain in the distal cavity.

It cannot be excluded that the presence of BHA in the H42E crystal structure determines which Glu42 side-chain O atom is protonated at this pH. Consequently, the proton could be located on $O^{\varepsilon1}$ in the uncomplexed enzyme, conserving the wild-type Asn70 side-chain conformation.

The R38S/H42E mutant structure shows that the absence of the Arg38 side chain has several interesting structural consequences (Fig. 3). The C18–C20 haem edge is displaced 0.5 Å away from the proximal side and into the distal pocket compared with the wild-type HRPC–FA structure (Henriksen *et al.*, 1999; Fig. 3*c*). Electron transfer from phenolic reducing substrates to the haem group in compound I is believed to occur at this edge (Ator & Ortiz de Montellano, 1987). The haem displacement is accompanied by a change in the position of the Phe221 side chain situated on the proximal side just below this part of the haem. The proximal haem ligand (His170) moves only insignificantly in the direction of the haem. Since the same movement was not observed for the opposite haem edge (C8–C10), the movement of the haem iron is less pronounced and the His170 $N^{\varepsilon2}$–iron distance differs by less than 0.18 Å in the two structures. This haem rearrangement is not only a translation, as illustrated by the relatively small dislocation of C3 and the C13 propionate in Fig. 3(*c*). Since the C8–C10 edge, C3 and the C13 propionate are moved only slightly while the C18–C20 edge is moved significantly, the shape of the haem porphyrin ring has changed. The haem group thus becomes slightly more saddle-shaped in the R38S/H42E mutant.

The main result of the R38S mutation is that the Glu42 side chain points in a completely different direction compared with the H42E structure (Figs. 2*b* and 3*b*). This has the effect that Asn70 moves down into the distal cavity (C^{α} moves 0.4 and 0.3 Å relative to the wild-type HRPC–FA and H42E structures, respectively; Fig. 3*c*) to optimize the hydrogen bond between the Asn70 and Glu42 side chains (2.6 Å; Fig. 3*b*). In this case, there is no evidence of a flipping of the Asn70 side-chain amide group. The rate of compound I formation of the R38S/H42E mutant is $3.2 \times 10^{1}\ M^{-1}\ s^{-1}$ (Smith & Veitch, 1998), which is comparable to that observed in the H42Q HRPC mutant ($k_1 = 9.6 \times 10^{1}\ M^{-1}\ s^{-1}$; Tanaka *et al.*, 1997). This, together with the observation that R38L HRPC has a k_1 value of $1.1 \times 10^{4}\ M^{-1}s^{-1}$ (Rodriguez-Lopez *et al.*, 1996*a*), implies that the proton acceptor in the distal cavity has been deactivated at pH 7.0 (the standard pH value for measuring compound I formation). Consequently, Glu42 is protonated in R38S/H42E under conditions where it is capable of accepting a proton in the H42E mutant. In R38S/H42E the Glu42 $O^{\varepsilon1}$ atom has no hydrogen-bonding contacts that could favour placement of the proton on this O atom. The proton is therefore likely to be placed on Glu42 $O^{\varepsilon2}$, which can then donate a hydrogen bond to the $O^{\delta1}$ atom in residue Asn70. In this way, Asn70 can in turn donate a hydrogen bond from the $N^{\delta2}$ atom to the Glu64 backbone O atom (2.9 Å) as in the wild-type enzyme, thereby preserving the wild-type Asn70 conformation (Fig. 3). This hypothesis is supported by the presence of the water molecule (WM3) coordinating to the distal calcium ion in R38S/H42E, which suggests that the wild-type distal side hydrogen-bonding network is preserved, in contrast to the situation in H42E, where WM3 is absent (see §3.3). A plausible explanation for the suggested lower acidity of Glu42 in R38S/H42E is that a charge on this side chain is energetically unfavourable because of the lack of the positive charge on Arg38 and the resulting lower polarity of the distal haem pocket. This idea is in accordance with the observation that the pK_a value of His42 in HRPC is approximately 2.5 (Dunford, 1999), which suggests the need for a non-charged base at position 42 in the distal cavity even in the presence of Arg38.

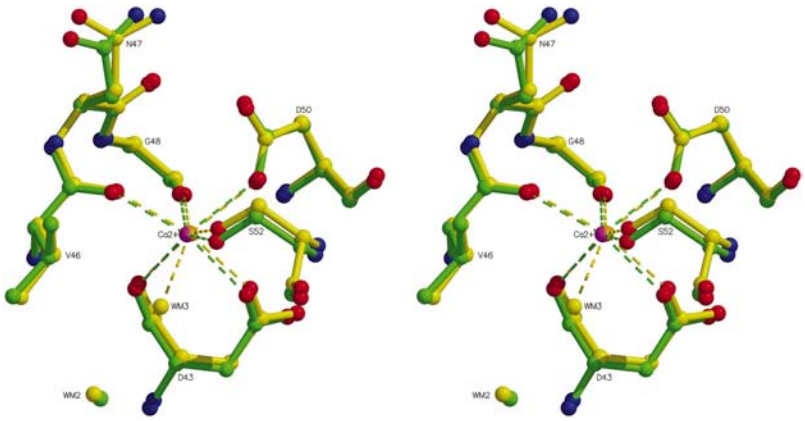

Figure 4
The distal calcium site in the wild-type HRPC–BHA (Henriksen *et al.*, 1998) and H42E structures. Only the amino acids coordinating to the calcium ion are shown. C atoms are in yellow and green for the wild type and H42E, respectively. The wild-type calcium ion is in orange, while the R38S/H42E calcium ion is in magenta. The water molecules and the coordination bonds (broken lines) have the same colour as the C atoms in the corresponding structure. VM3 is absent in H42E. Residues are labelled with single-letter codes. This figure was produced with the programs *MOLSCRIPT* (Kraulis, 1991) and *RASTER3D* (Merritt & Murphy, 1994).

The difference in the position of the Glu42 side chain in the H42E and R38S/H42E mutants is probably caused by the greater intrinsic flexibility of glutamic acid compared with histidine, combined with the fewer steric constraints owing to the smaller side chain at position 38. Furthermore, WM1 normally present between the distal histidine and the haem iron is missing in R38S/H42E. WM1 is observed in the wild-type structures both with and without bound substrates (BHA and FA; Gajhede *et al.*, 1997; Henriksen *et al.*, 1998, 1999), where it is hydrogen bonded to His42 and Arg38 (Figs. 2*a* and 3*a*). In the absence of the Arg38 side chain WM1 is no longer fixed at this position, which in turn removes a stabilizing hydrogen bond to the Glu42 side chain. This causes it to reorient to a more favourable position and diminishes the chance that Glu42 will be correctly positioned for catalysis in the distal

cavity of R38S/H42E (Fig. 3*b*). The position of Glu42 in the H42E crystal structure is probably also constrained by the presence of BHA in the distal cavity.

The absence of the bulky Arg38 side chain and the resulting movement of the Glu42 side chain also have consequences for the surrounding residues. The Phe41 phenyl ring moves towards the vacant distal pocket (0.6 Å; Fig. 3*c*). Furthermore, Ser73, which in the wild type is hydrogen bonded to Arg38 $N^{\eta1}$ and $N^{\eta2}$ and the C17 haem propionate, is rotated and hydrogen bonds to the same haem propionate and to the backbone O atoms of residues 71 and 72. This suggests that the C17 haem propionate is protonated in the R38S/H42E structure.

No FA is observed in the distal cavity in the R38S/H42E structure, implying that the properties of the cavity have changed sufficiently to impair FA binding. The absence of the FA1 and FA3 binding modes observed in the wild-type HRPC–FA structure is readily explained by the lack of the Arg38 side chain, which hydrogen bonds to both of these. The FA2 binding mode is on the other hand only stabilized by a hydrogen bond to Pro139 and this residue is unaffected by the mutations. Except for Phe179, none of the hydrophobic residues lining the entrance to the distal cavity are displaced by the mutations compared with the wild-type structure (Fig. 3*c*). The absent FA2 molecule could therefore indicate that the reducing substrate-binding properties depend not only on specific hydrogen bonds, but also on overall electrostatic effects.

3.3. Distal side hydrogen-bonding network

The calcium ion present on the distal side of the haem is seven-coordinated in all three wild-type HRPC structures (Gajhede *et al.*, 1997; Henriksen *et al.*, 1998, 1999), with six amino-acid ligands and the water molecule denoted WM3 as the seventh ligand. WM3 is very well ordered, with a *B* factor of less than 12 $Å^2$ in these structures. There is no electron density at this position in the H42E structure, not even if WM3 is included in the model during the map calculation; consequently, there is no experimental evidence for the presence of WM3. No other atoms have moved to fill the vacant ligand site and the result is a six-coordinated calcium ion (Fig. 4). The coordination geometry has therefore changed from a pentagonal bipyramid to a distorted octahedron. Interestingly, WM3 is present in the R38S/H42E structure. The reason why WM3 is missing in the H42E structure but present in R38S/H42E could be a difference in the orientation of the Asn70 side chain in the two mutant structures, as discussed in §3.2. If the proton on the Glu42 side-chain carboxylic acid is located on $O^{\varepsilon2}$ in H42E, it causes the flipping of the Asn70 side-chain amide group so it can donate a hydrogen bond to Glu42. As a result, the position occupied by Asn70 $N^{\delta2}$ in the wild type becomes occupied by Asn70 $O^{\delta1}$. This disturbs the hydrogen-bonding network extending from the Asn70 side chain to WM3 (*via* the Glu64 side chain and backbone O atom, the residue 42 backbone O atom and WM2), resulting in the absence of WM3 (Fig. 5). According to the argumentation in §3.2, there is no reason to believe that Glu42 is not capable of donating a hydrogen bond to the Asn70 side chain in R38S/H42E. In this situation the Asn70 $O^{\delta1}$ atom points towards the distal cavity, thereby preserving the wild-type distal hydrogen-bonding network and the WM3 water molecule.

This theory is supported by the proposed mechanism for the catalytic cycle of CPO (Sundaramoorthy *et al.*, 1998), where a hydrogen bond between the protonated His105 side chain and the catalytic base Glu183 keeps this glutamic acid in the correct orientation and modulates its acidity, so it can act as a proton acceptor during compound I formation. The same would be true in the active state of the H42E mutant if the Asn70 amide side chain is flipped as proposed here, which would explain

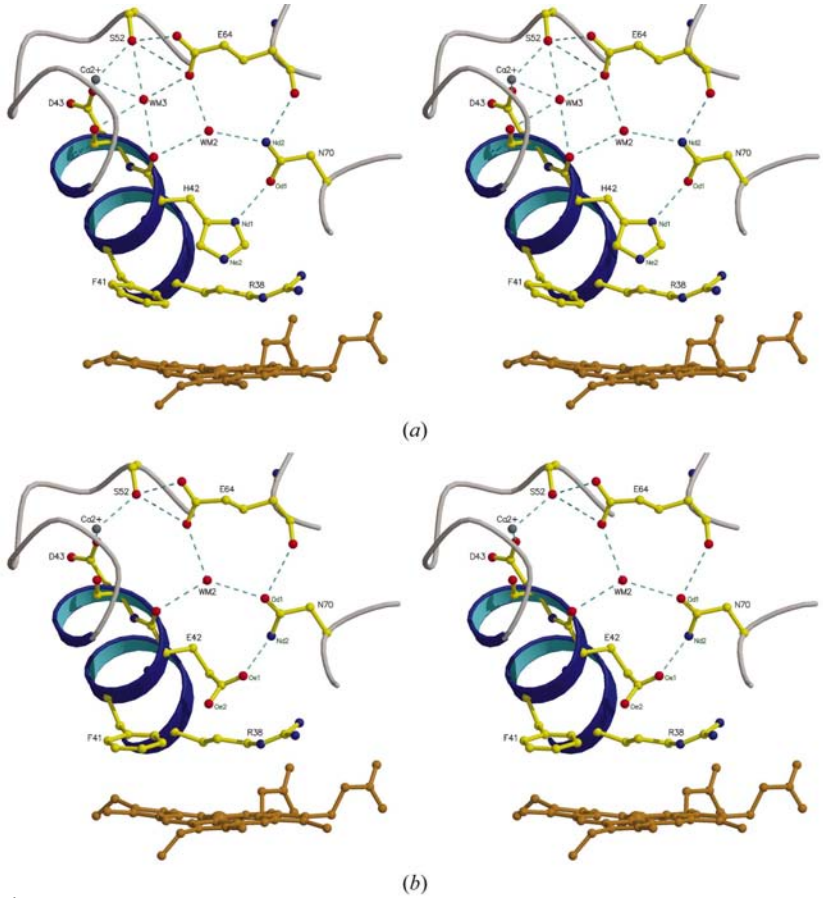

Figure 5
The hydrogen-bonding network connecting residue 42 to the distal calcium ion in (*a*) the wild-type HRPC–BHA (Henriksen *et al.*, 1998) and (*b*) H42E structures. Hydrogen bonds with a maximum length of <3.5 Å between selected atoms are shown by broken lines. Residues are labelled with single-letter codes. In the atom names d = δ and e = ε. This figure was produced with the programs *MOLSCRIPT* (Kraulis, 1991) and *RASTER3D* (Merritt & Murphy, 1994).

why k_1 is 50 times higher compared with the H42Q HRPC mutant (Tanaka *et al.*, 1997). The conclusions drawn from the mutant structures suggest that the hydrogen-bonding network from His42 to the distal calcium ion including the two water molecules WM2 and WM3 helps to assure that the Asn70 and therefore the His42 side chains are in the optimal conformations for catalysis.

There is another possible explanation for the missing WM3 water molecule in H42E. In all figures with superimposed structures, the structures are superimposed using *O* (Jones *et al.*, 1991), with a least-squares calculation minimizing the distance between corresponding C^{α} atoms for residues 1–306. When the H42E and HRPC–BHA structures are superimposed in this way, the residue 42 backbone O atom is further away from the distal calcium site in H42E compared with the wild type. The His42 O–WM3 distance is 2.9 Å, while the distance from Glu42 O to the equivalent position is 3.2 Å. The hydrogen bond to a water molecule placed in exactly this position in the H42E crystal structure would therefore be weaker. It is not possible to calculate whether this difference changes the energy of the system enough to make the binding of WM3 unfavourable when taking into account that the extensive interactions with Asp43, Glu64, Ser52 and the calcium ion are lost (Fig. 5). Since the discrepancy is relatively small and in the same order as the coordinate error, the choice of atoms used for the least-squares calculation during the superposition has important consequences. If the calculation is performed using only the C^{α} atoms for the residues surrounding the distal calcium ion (residues 44–53), the distance from Glu42 O to the HRPC–BHA WM3 site is reduced to 3.1 Å. It is thus possible that the longer distance is insignificant and that the effect on the Glu42 O–WM3 interaction would be negligible if WM3 was present. Anyway, this possibility cannot be excluded on the basis of the structural data.

4. Conclusions

A comparison of the crystal structure of the H42E–BHA complex with that of the corresponding wild-type BHA complex shows that the side-chain O atoms of Glu42 occupy positions very similar to the $N^{\delta1}$ and $N^{\varepsilon2}$ atom positions of His42 in the wild type. Glutamic acid is intrinsically more flexible and has a smaller side-chain volume, but its position is constrained by a hydrogen bond to Asn70, a residue that is important for catalysis in the wild-type enzyme. The Asn70 side-chain amide group is rotated 180° so it can donate a hydrogen bond to Glu42, which is suggested to be protonated on the side-chain O atom interacting with BHA and a water molecule located immediately above the haem. Consequently, Glu42 can function as a proton acceptor during catalysis if the pH is high enough to allow it to be deprotonated. The rotation of Asn70 disturbs the hydrogen-bonding network on the distal side of the haem. This results in the absence of the water molecule serving as the seventh ligand to the distal calcium ion in wild-type HRPC.

No FA molecules are observed in the distal cavity of the R38S/H42E structure. This indicates that the binding of phenolic reducing substrates is less favourable, which presumably slows the reduction of any compound I or compound II formed by this mutant. Furthermore, the absence of Arg38 causes Glu42 to be relocated and to be protonated on the side-chain O atom hydrogen bonding to Asn70 in the resting enzyme, thereby preserving the Asn70–residue 42 interaction. This results in improper positioning of Glu42 in the distal cavity and makes it impossible for glutamic acid to substitute for the usual proton acceptor in the catalytic cycle. This substitution of the distal histidine is only possible if Arg38 is present to limit the flexibility and modulate the acidity of Glu42.

This work was supported by the Danish Natural Research Council through the DANSYNC grant, by EU contract BIO4-97-2031 'Towards Designer Peroxidases' to MG and ATS, and by the BBSRC (B17590) to ATS. We would like to thank ESRF (ID-14) for providing synchrotron beam time.

References

Ator, M. A. & Ortiz de Montellano, P. R. (1987). *J. Biol. Chem.* **262**, 1542–1551.
Berglund, G. I., Carlsson, G. H., Smith, A. T., Szoke, H., Henriksen, A. & Hajdu, J. (2002). *Nature (London)*, **417**, 463–468.
Brünger, A. T. (1992*a*). *Nature (London)*, **355**, 472–475.
Brünger, A. T. (1992*b*). *X-PLOR Version 3.1. A System for X-ray Crystallography and NMR.* New Haven, CT, USA: Yale University Press.
Brünger, A. T., Adams, P. D., Clore, G. M., DeLano, W. L., Gros, P., Grosse-Kunstleve, R. W., Jiang, J. S., Kuszewski, J., Nilges, M., Pannu, N. S., Read, R. J., Rice, L. M., Simonson, T. & Warren, G. L. (1998). *Acta Cryst.* D**54**, 905–921.
Brünger, A. T., Adams, P. D. & Rice, L. M. (1997). *Structure*, **5**, 325–336.
Burmeister, W. P. (2000). *Acta Cryst.* D**56**, 328–341.
Dunford, H. B. (1991). *Peroxidases in Chemistry and Biology*, edited by J. Everse & M. B. Grisham, pp. 1–24. Boca Raton: CRC Press.
Dunford, H. B. (1999). *Heme Peroxidases.* New York: John Wiley & Sons.
Edwards, S. L., Nguyen, H. X., Hamlin, R. C. & Kraut, J. (1987). *Biochemistry*, **26**, 1503–1511.
Engh, R. A. & Huber, R. (1991). *Acta Cryst.* A**47**, 392–400.
Fülöp, V., Phizackerley, R. P., Soltis, S. M., Clifton, I. J., Wakatsuki, S., Erman, J., Hajdu, J. & Edwards, S. L. (1994). *Structure*, **2**, 201–208.
Gajhede, M. (2001). *Biochem. Soc. Trans.* **29**, 91–98.
Gajhede, M., Schuller, D. J., Henriksen, A., Smith, A. T. & Poulos, T. L. (1997). *Nature Struct. Biol.* **4**, 1032–1038.
Henriksen, A., Schuller, D. J., Meno, K., Welinder, K. G., Smith, A. T. & Gajhede, M. (1998). *Biochemistry*, **37**, 8054–8060.
Henriksen, A., Smith, A. T. & Gajhede, M. (1999). *J. Biol. Chem.* **274**, 35005–35011.
Jiang, J. S. & Brünger, A. T. (1994). *J. Mol. Biol.* **243**, 100–115.
Jones, T. A., Zou, J.-Y., Cowan, S. W. & Kjeldgaard, M. (1991). *Acta Cryst.* A**47**, 110–119.
Kleywegt, G. J. & Brünger, A. T. (1996). *Structure*, **4**, 897–904.
Kraulis, P. J. (1991). *J. Appl. Cryst.* **24**, 946–950.
Laskowski, R. A., Macarthur, M. W., Moss, D. S. & Thornton, J. M. (1993). *J. Appl. Cryst.* **26**, 283–291.
Merritt, E. A. & Murphy, M. E. P. (1994). *Acta Cryst.* D**50**, 869–873.

Mukai, M., Nagano, S., Tanaka, M., Ishimori, K., Morishima, I., Ogura, T., Watanabe, Y. & Kitagawa, T. (1997). *J. Am. Chem. Soc.* **119**, 1758–1766.
Nagano, S., Tanaka, M., Ishimori, K., Watanabe, Y. & Morishima, I. (1996). *Biochemistry*, **35**, 14251–14258.
Newmyer, S. L. & Ortiz de Montellano, P. R. (1996). *J. Biol. Chem.* **271**, 14891–14896.
Otwinowski, Z. (1993). *Proceedings of the CCP4 Study Weekend. Data Collection and Processing*, edited by L. Sawyer, N. Isaacs & S. Bailey, pp. 56–62. Warrington: Daresbury Laboratory.
Pannu, N. S. & Read, R. J. (1996). *Acta Cryst.* A**52**, 659–668.
Poulos, T. L. & Kraut, J. (1980). *J. Biol. Chem.* **255**, 8199–8205.
Read, R. J. (1986). *Acta Cryst.* A**42**, 140–149.
Rodriguez-Lopez, J. N., Smith, A. T. & Thorneley, R. N. F. (1996*a*). *J. Bioinorg. Chem.* **1**, 136–142.
Rodriguez-Lopez, J. N., Smith, A. T. & Thorneley, R. N. F. (1996*b*). *J. Biol. Chem.* **271**, 4023–4030.
Savenkova, M. I., Kuo, J. M. & Ortiz de Montellano, P. R. (1998). *Biochemistry*, **37**, 10828–10836.
Savenkova, M. I., Newmyer, S. L. & Ortiz de Montellano, P. R. (1996). *J. Biol. Chem.* **271**, 24598–24603.
Smith, A. T., Sanders, S. A., Sampson, C., Bray, R. C., Burke, J. F. & Thorneley, R. N. F. (1993). *Plant Peroxidases, Biochemistry and Physiology*, edited by K. G. Welinder, S. K. Rasmussen, C. Penel & H. Greppin, pp. 159–168. University of Geneva Press.
Smith, A. T., Sanders, S. A., Thorneley, R. N. F., Burke, J. F. & Bray, R. R. C. (1992). *Eur. J. Biochem.* **207**, 507–519.
Smith, A. T., Santama, N., Daceys, S., Edwards, M., Bray, R. C., Thorneley, R. N. F. & Burke, J. F. (1990). *J. Biol. Chem.* **265**, 13335–13343.
Smith, A. T. & Veitch, N. C. (1998). *Curr. Opin. Chem. Biol.* **2**, 269–278.
Sun, W., Kadima, T. A., Pickard, M. A. & Dunford, H. B. (1994). *Biochem. Cell. Biol.* **72**, 321–331.
Sundaramoorthy, M., Terner, J. & Poulos, T. L. (1995). *Structure*, **3**, 1367–1377.
Sundaramoorthy, M., Terner, J. & Poulos, T. L. (1998). *Chem. Biol.* **5**, 461–473.
Tanaka, M., Ishimori, K. & Morishima, I. (1996). *Biochem. Biophys. Res. Commun.* **227**, 393–399.
Tanaka, M., Ishimori, K., Mukai, M., Kitagawa, T. & Morishima, I. (1997). *Biochemistry*, **36**, 9889–9898.